Optics Letters

Directly diode-pumped femtosecond Cr:ZnS amplifier with ultra-low intensity noise

Shizhen Qu,[1,2,3] **Arun Paudel,**[1,2,3] **Aleksandar Sebesta,**[1,2,3] **Philipp Steinleitner,**[3]
Nathalie Nagl,[2,3] **Markus Poetzlberger,**[3] **Vladimir Pervak,**[2] **Ka Fai Mak,**[3] **and**
Alexander Weigel[1,3,*]

[1]*Center for Molecular Fingerprinting, 1093 Budapest, Czuczor utca 2-10, Hungary*
[2]*Ludwig-Maximilians-Universität München, Am Coulombwall 1, 85748 Garching, Germany*
[3]*Max Planck Institute of Quantum Optics, Hans-Kopfermann-Str. 1, 85748 Garching, Germany*
Corresponding author: alexander.weigel@mpq.mpg.de

Diode-pumped Cr:ZnS oscillators have emerged as precursors for single-cycle infrared pulse generation with excellent noise performance. Here we demonstrate a Cr:ZnS amplifier with direct diode-pumping to boost the output of an ultrafast Cr:ZnS oscillator with minimum added intensity noise. Seeded with a 0.66-W pulse train at 50-MHz repetition rate and 2.4 μm center wavelength, the amplifier provides over 2.2 W of 35-fs pulses. Due to the low-noise performance of the laser pump diodes in the relevant frequency range, the amplifier output achieves a root mean square (RMS) intensity noise level of only 0.03% in the 10 Hz–1 MHz frequency range and a long-term power stability of 0.13% RMS over one hour. The diode-pumped amplifier reported here is a promising driving source for nonlinear compression to the single- or sub-cycle regime, as well as for the generation of bright, multi-octave-spanning mid-infrared pulses for ultra-sensitive vibrational spectroscopy. © 2022 Optica Publishing Group

Ultrafast laser systems based on Cr^{2+}-doped II–VI gain media have evolved into infrared alternatives to mature Ti:sapphire technology [1–3]. Mode-locked Cr:ZnS/ZnSe laser oscillators nowadays provide few-cycle pulses in the 2–3 μm spectral range [1,3–8], making them ideal sources to probe molecular and semiconductor systems, for example by dual-comb spectroscopy [9,10]. In addition, the emission wavelengths of Cr:ZnS/ZnSe oscillators provide optimum phase-matching conditions for further frequency downconversion in highly nonlinear crystals such as GaSe and $ZnGeP_2$, enabling the generation of multi-octave-spanning mid-infrared pulses with percent-level conversion efficiencies [11–14]. Refining the system further, we recently post-compressed the output of a carrier-envelope-phase (CEP) stable Cr:ZnS oscillator in a rutile plate, achieving true single-cycle pulses, and efficiently downconverted these pulses into controllable single-cycle mid-infrared waveforms [14]. A current limitation of ultrafast Cr:ZnS/ZnSe oscillators is still the achievable average output power, which can barely be scaled beyond the 1–2 Watt level [2]. Increasing the output power to

the multi-Watt level would provide the basis for even stronger nonlinear spectral broadening toward the visible, with sufficient bandwidth to reach the sub-cycle regime, and the potential to generate broadband mid-infrared pulses with > 100 mW average power. Such power scaling requires post-amplification of the oscillator output.

Laser pulse amplification in Cr:ZnS/ZnSe gain media has been demonstrated previously, reaching multiple Watts [15–18]. As pump sources for MHz-rate Cr:ZnS/ZnSe amplifiers, up to now only fiber lasers doped with rare-earth elements like erbium [15,16] or thulium [18] have been used. These lasers conveniently provide high pump powers in the relevant absorption bands, combined with diffraction-limited output beams. Recently, single-emitter laser diodes have evolved as promising alternatives for oscillator pumping, reaching ultra-low noise performance [8,14]. Their relaxation oscillation noise spikes at GHz frequencies, so that it is averaged out within the Cr^{2+} upper-state lifetime [19]. Together with their compactness, high wall-plug efficiency, and cost effectiveness, they are ideal pump sources for low-noise infrared laser applications. Diode-pumped Cr:ZnS/ZnSe oscillators have been demonstrated in both continuous-wave [20] and mode-locked operation [7,8]. A recent laser system combining a diode-pumped, Kerr-lens mode-locked oscillator with nonlinear post-compression achieved 7.7-fs, single-cycle pulses with an intensity noise of only 0.04% root mean square (RMS), integrated over the 10 Hz to 1 MHz range [14]. Despite their success for oscillator pumping, their limitations in output power and beam quality prevented up to now the use of laser diodes for pumping Cr:ZnS/ZnSe amplifiers.

Here we report the first directly diode-pumped Cr:ZnS amplifier, providing 2.2 W of 35-fs pulses (4.4 optical cycles) at 50-MHz repetition rate and 2.4 μm center wavelength. Combining four laser diodes provided the required pump power for amplification. Despite the poor pump-beam quality, we achieved power extraction with a slope efficiency of 18% by employing a bow-tie shaped triple-pass amplification scheme, folded in the plane of strongest pump-beam divergence. The key feature of the amplifier system is its ultra-low noise performance, with a relative intensity noise (RIN) for the output of only 0.03% RMS in the range from 10 Hz to 1 MHz—one of the lowest values for
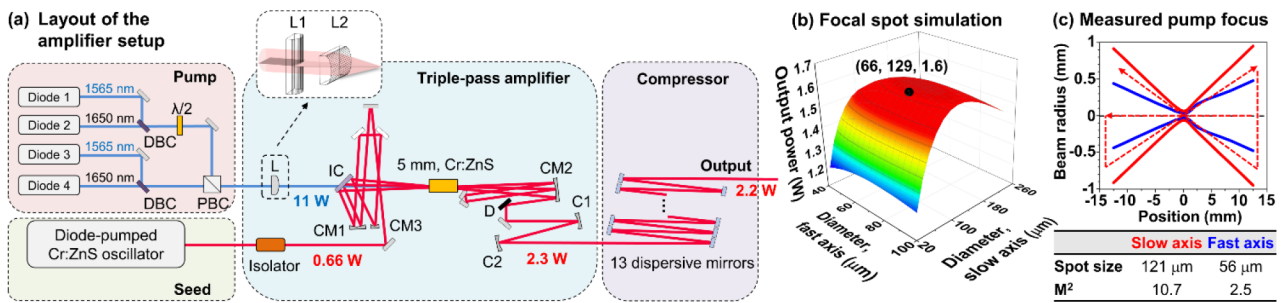
Fig. 1. (a) Layout of the diode-pumped Cr:ZnS amplifier. DBC, dichroic beam combiner; PBC, polarization beam combiner; CM, curved mirrors (CM1, CM3: f = 100 mm; CM2: f = 150 mm); IC, input coupler; $\lambda/2$, half-wave plate; L, cylindrical lens group (L1: f = 150 mm; L2: f = 75 mm); C, cylindrical mirrors (C1: f = 100 mm; C2: f = 50 mm); D, pickup mirror. (b) Simulated single-pass output power, depending on the pump focal spot dimensions, with an optimum found for a focal spot of 129 µm × 66 µm along slow and fast axes, respectively. (c) Measured caustic of the pump beam around the crystal position along slow and fast axes, and focal spot diameters ($1/e^2$). The seed-beam folding is indicated by dashed red arrows.

Cr:ZnS/Se lasers reported so far. The amplifier is not reaching pump saturation under our conditions and allows further power scaling with, e. g., higher-brightness laser diodes in the future.

The layout of the diode-pumped Cr:ZnS amplifier is shown in Fig. 1(a). The seed laser of the amplifier is a diode-pumped, Kerr-lens mode-locked, femtosecond Cr:ZnS oscillator, similar to the one reported by Nagl *et al*. in Ref. [7,8]. The oscillator provides up to 0.78 W of average power at a repetition rate of 50 MHz and a central wavelength of 2.4 µm. The output pulses directly from the oscillator pass through a Faraday isolator with 85% transmission, leaving 0.66 W for seeding the amplifier. The seed is focused by a curved mirror (CM1) to a round focal spot of 64 µm diameter ($1/e^2$) and combined with the pump beam via a plane input coupler (IC) with 45° angle of incidence.

Four InP single-emitter laser diodes (SemiNex Corporation), two emitting at 1.65 µm and two at 1.565 µm, are pumping the amplifier. Since the output power of each single-emitter diode is limited to below 3.5 W, we combined the four diodes into a single beam with 11 W pump power via wavelength and polarization multiplexing [21,22], using dichroic beam combiners (DBCs), a wave plate ($\lambda/2$), and a polarizing beam combiner (PBC). M^2 values of 2.5 along the fast axis and 10.7 along the slow axis were measured for the combined beam with a scanning-slit beam profiler (Ophir, NanoScan). The anisotropic pump beam is focused with two cylindrical lenses (L1 and L2) into the 5-mm-thick polycrystalline Cr:ZnS gain crystal (IPG, $\sim 7 \times 10^{18}$ cm^{-3} doping concentration) [8,22]. We chose Cr:ZnS due to its superior thermal conductivity and smaller temperature dependence of the refractive index compared to Cr:ZnSe [2,15]. The optimum focusing conditions for amplification were studied via simulations with the commercial software ASLD [23] [Fig. 1(b)]. Using our experimental parameters, we found in the simulation the highest single-pass amplification for a pump focus of 129 µm (slow axis) × 66 µm (fast axis). Based on the simulation, we adjusted the diode collimation and the cylindrical lenses L1 and L2 and achieved an experimentally measured pump spot size of 121 µm (slow axis) × 56 µm (fast axis) at the crystal position.

In order to efficiently extract energy from the strongly divergent pump beam, the seed is sent three times through the gain medium, folded in a bow-tie arrangement in the plane of the slow axis of the pump beam [Fig. 1(c), red dashed arrows]. The larger divergence and spot size of the pump beam along this axis favorably support the overlap with the three noncollinear seed

beam passes in the crystal. The triple-pass geometry boosts the seed power to 1.6 W, 2 W, and 2.3 W after the 1st, 2nd, and 3rd pass, respectively, using only a single-gain crystal. Given the gain saturation under our conditions, we do not expect further increase in output power beyond about 2.4 W by adding additional passes through the gain medium. The amplified seed beam is picked up after the third pass with a D-shaped silver mirror (D) and sent into a cylindrical mirror telescope (C1 and C2) to correct for spatial distortions. After that, a compressor consisting of a combination of complementary chirped-mirror pairs and third-order dispersion mirrors, corrects for the accumulated group-delay dispersion and third-order dispersion [24]. The main contributions to temporal dispersion in our case were the output coupler and output window of the oscillator, the Faraday isolator, and the Cr:ZnS amplifier gain crystal.

The total output power after the compressor is 2.2 W, corresponding to an overall gain factor of 3.3. The output power depends linearly on the absorbed pump power [Fig. 2(a)], without reaching a power roll-off due to thermal or other effects [25]. The slope efficiency of amplification is 18%. Changing the input seed power after the Faraday isolator from 0.1 to 0.66 W increases the amplifier output power (black) from 1.1 to 2.2 W [Fig. 2(b)]. Simultaneously, the gain factor (blue) decreases from 9 to 3.3 at the full absorbed pump power of 9.7 W, indicating a saturation of the optical gain with the available pump power.

The output spectrum of the amplifier, measured with a rotating-grating-based spectrometer (APE GmbH, WaveScan), is shown in Fig. 3(a) (red). The spectrum spans from 2 µm to ~ 2.7 µm, at the −30-dB level. When comparing the spectra of seed and amplified pulses, only around 1% of spectral narrowing is observed for the full width at half maximum (FWHM)—see
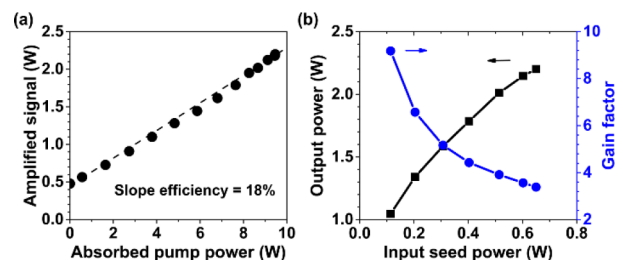

Fig. 2. (a) Amplifier output power, depending on the absorbed pump power (black dots), and linear fit (dashed line). (b) Output power (black) and gain factor (blue) versus seed power.
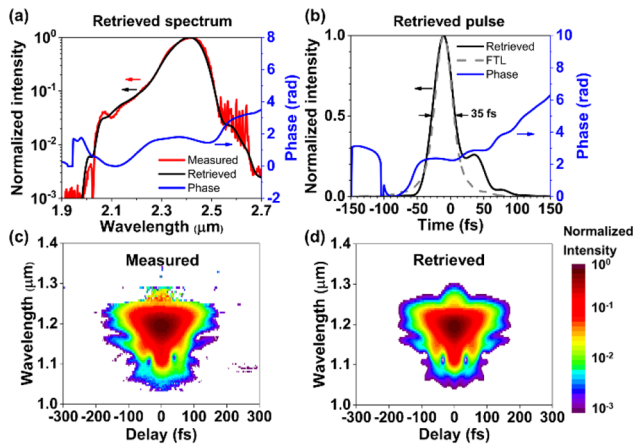
Fig. 3. Characterization of the amplifier output pulses with frequency-resolved optical gating (FROG). (a) Measured and retrieved spectra and retrieved spectral phase. (b) Retrieved pulse shape (35 fs FWHM), temporal phase, and Fourier-transform-limited (FTL) pulse. (c) Measured, and (d) retrieved FROG traces.

Fig. 4. Beam quality measurement after the cylinder telescope for tangential (blue dots) and sagittal directions (black dots), together with hyperbolic fits (solid curves) and extracted M^2 values. Inset: output beam profile measured after the cylindrical telescope.

Fig. S5 in the Supplement 1. We ascribe the maintained spectral bandwidth to the balancing of the amplification-induced narrowing by the slight spectral broadening due to self-phase modulation in the Cr:ZnS gain crystal. Strong spectral broadening as reported by Vasilyev *et al.* in Ref. [16] was not observed in this experiment, consistent with an estimated B integral of $< \pi/6$. In the range from 2.5 to 2.7 µm the spectrum shows several sharp features from CO_2 and water absorption in the oscillator. The amplifier output spectrum supports a 32-fs Fourier-transform-limited (FTL) pulse duration.

The compressed pulses were temporally characterized with a home-built frequency-resolved optical gating (FROG) device, using a 100-µm-thick $LiIO_3$ crystal for second harmonic generation. Figures 3(c) and 3(d) show the measured and retrieved FROG traces on a logarithmic axis, with a retrieval error of 0.36%. The retrieved spectrum [black in Fig. 3(a)] matches the measured spectrum [red in Fig. 3(a)]. The retrieved pulse [black in Fig. 3(b)] has a FWHM duration of 35 fs, corresponding to 4.4 optical cycles, only 10% longer than the transform-limited pulse [dashed gray in Fig. 3(b)]. Some smaller sidelobes result from higher-order dispersion.

The amplified seed beam, while having excellent focusing properties, is elongated along the tangential direction. We attribute the change in beam profile during amplification to the asymmetric gain region. Another contribution may arise from non-symmetric thermal lensing in the gain medium [2] due to different cooling efficiencies for the crystal along tangential and sagittal directions. We correct the change in beam shape with a telescope consisting of two cylindrical silver mirrors (Thorlabs), leading to the round far-field beam profile shown as an inset to Fig. 4. The focusing properties of the beam after the cylinder telescope were characterized with a scanning-slit beam profiler (Ophir, Nanoscan, Fig. 4). We found the values of M^2 to be 1.09 and 1.06 in the tangential and sagittal directions, respectively, indicating a close-to-diffraction-limited focusing behavior for the amplifier output beam. The beam quality is consistent with an estimated B integral $< \pi/6$.

The intensity noise behaviors of the seed and amplifier outputs were measured with a biased InGaAs photodetector (Thorlabs, DET10D2), with voltage post-amplification (Stanford Research
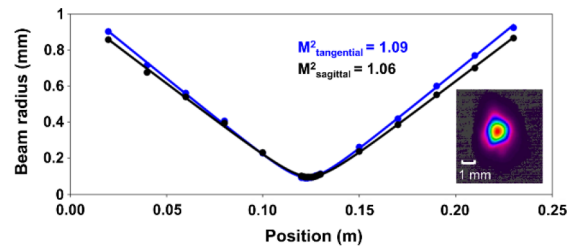
Systems, SRS560), connected to a fast data acquisition card (GaGe, Razor 16) for digitization. Figure 5(a) shows the RIN, obtained from the measured time-domain data via Fourier transformation. Above 10 Hz [Fig. 5(a), right], the resulting RIN curve of the amplifier (red) closely resembles that of the seed laser (black). Both curves show a typical 1/f behavior below 1 kHz [26], with spikes from low-frequency vibrations and electrical noise, followed by a plateau region in the range 1 to 100 kHz, and a noise peak at 600 kHz from relaxation oscillations of the seed laser. Above 600 kHz, the noise curve gradually drops to the background noise level (gray). Higher-frequency noise components of the pump laser diodes are strongly damped due to the microsecond upper-state lifetime of the Cr:ZnS gain media, both in the oscillator and in the amplifier, so that we expect close-to-quantum-noise-limited behavior above 1 MHz (see Fig. S4a in the Supplement 1) [27]. A small increase of the RIN by a few decibels is observed with amplification in the plateau region in the range 1–200 kHz, which can be attributed to additional white noise from the amplifier pump diodes. Another small increase in RIN is observed for the amplifier output at low frequencies around 100 Hz, which we attribute to mechanical vibrations in the amplifier setup. By integrating the RIN, we obtained for the amplifier output an RMS intensity noise of only 0.03% in the 10 Hz to 1 MHz range. Amplification increases the intensity noise in this frequency range only by a factor of 1.03, demonstrating the potential of diode-pumped amplification for ultra-low noise applications. The corresponding RIN from 10^{-4} Hz to 10 Hz is shown in the left panel of Fig. 5(a), and the originally measured time-domain power fluctuations over one hour are compared in Fig. 5(b). We find for the entire frequency range spanning from 10^{-4} Hz to 1 MHz, integrated RMS intensity noise values of 0.09% and 0.13% for the seed and amplifier, respectively. We attribute the slight increase in noise below 1 Hz for the amplified output to mechanical vibrations and beam-pointing fluctuations, which can be reduced in future by mechanical optimization of the amplifier. We attribute the overall excellent noise performance of the amplifier to the use of laser diodes for pumping, with some possible minor contributions from gain saturation. Note that due to the lack of reported data we cannot compare our noise performance to that of previously published Cr:ZnS/ZnSe amplifiers with fiber-pumped sources, but our result rivals the best noise performances reported for Cr:ZnS/Se oscillators alone [8,14,28–31].

In conclusion, we demonstrated an ultra-low noise, femtosecond diode-pumped Cr:ZnS amplifier. Driven by four single-emitter laser diodes, the amplifier provides 2.2 W of output power and 35-fs pulses at a central wavelength of 2.4 µm. The amplifier complements the previously reported
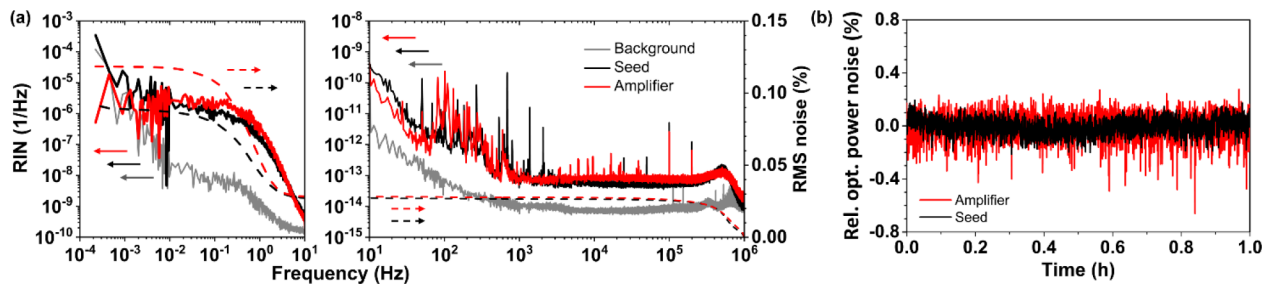
Fig. 5. (a) Relative intensity noise (RIN, full curves) of the seed, the amplifier output, and the detection-noise background. Dashed curves: corresponding integrated RMS intensity noises. (b) Long-term relative power fluctuations of the amplifier and oscillator seed in the time domain.

diode-pumped Cr:ZnS oscillators [7,8] in boosting the average power to the multi-Watt level, while maintaining ultra-low noise performance. With our amplifier system, we reached an integrated intensity noise of only 0.03% RMS in the 10 Hz to 1 MHz range and 0.13% in the 10^{-4} Hz to 1 MHz range. The dependence of the amplified output power on absorbed pump power is linear, without reaching a power roll-off at our pump levels. Therefore, we see the potential for further power scaling by adding more laser diodes or using more powerful single-emitter diodes in the future [32]. Combined with nonlinear post-compression [14], the diode-pumped Cr:ZnS amplifier system can be extended into a powerful and highly stable source for single- or even sub-cycle pulses at infrared wavelengths. Further cascaded downconversion will provide multi-octave-spanning mid-infrared pulses [11–14] with unprecedented brightness and ultra-low intensity noise—ideal for ultra-sensitive spectroscopic applications.

Disclosures. The authors declare no conflicts of interest.

Data availability. Data underlying the results presented in this paper are not publicly available at this time but may be obtained from the authors upon reasonable request.

Supplemental document. See Supplement 1 for supporting content.

REFERENCES

1. I. T. Sorokina and E. Sorokin, IEEE J. Sel. Top. Quantum Electron. **21**, 273 (2015).
2. S. B. Mirov, I. S. Moskalev, S. Vasilyev, V. Smolski, V. V. Fedorov, D. Martyshkin, J. Peppers, M. Mirov, A. Dergachev, and V. Gapontsev, IEEE J. Sel. Top. Quantum Electron. **24**, 1 (2018).
3. S. Vasilyev, I. Moskalev, M. Mirov, V. Smolski, S. Mirov, and V. Gapontsev, Opt. Mater. Express **7**, 2636 (2017).
4. A. Barh, J. Heidrich, B. Alaydin, M. Gaulke, M. Golling, C. R. Phillips, and U. Keller, Opt. Express **29**, 5934 (2021).
5. J. G. Meyer and O. Pronin, in *2021 CLEO/Europe-EQEC* (Optica Publishing Group, 2021), pp. 1.
6. M. N. Cizmeciyan, H. Cankaya, A. Kurt, and A. Sennaroglu, Opt. Lett. **34**, 3056 (2009).
7. N. Nagl, S. Grobmeyer, M. Potzlberger, V. Pervak, F. Krausz, and K. F. Mak, in *CLEO* (Optica Publishing Group, 2020), pp. SF3H–5.
8. N. Nagl, S. Gröbmeyer, V. Pervak, F. Krausz, O. Pronin, and K. F. Mak, Opt. Express **27**, 24445 (2019).
9. S. Vasilyev, V. Smolski, J. Peppers, I. Moskalev, M. Mirov, Y. Barnakov, S. Mirov, and V. Gapontsev, Opt. Express **27**, 35079 (2019).
10. B. Bernhardt, E. Sorokin, P. Jacquet, R. Thon, T. Becker, I. T. Sorokina, N. Picqué, and T. W. Hänsch, Appl. Phys. B **100**, 3 (2010).
11. S. Vasilyev, I. S. Moskalev, V. O. Smolski, J. M. Peppers, M. Mirov, A. V. Muraviev, K. Zawilski, P. G. Schunemann, S. B. Mirov, K. L. Vodopyanov, and V. P. Gapontsev, Optica **6**, 111 (2019).
12. N. Nagl, V. Pervak, F. Krausz, and K. F. Mak, in *CLEO/Europe-EQEC* (Optica Publishing Group, 2021), pp. cf_6_1.
13. Q. Wang, J. Zhang, A. Kessel, N. Nagl, V. Pervak, O. Pronin, and K. F. Mak, Opt. Lett. **44**, 2566 (2019).
14. P. Steinleitner, N. Nagl, M. Kowalczyk, J. Zhang, V. Pervak, C. Hofer, A. Hudzikowski, J. Sotor, A. Weigel, F. Krausz, and K. F. Mak, Nat. Photonics **16**, 512 (2022).
15. S. Vasilyev, I. Moskalev, M. Mirov, S. Mirov, and V. Gapontsev, Opt. Express **24**, 1616 (2016).
16. S. Vasilyev, I. Moskalev, V. Smolski, J. Peppers, M. Mirov, V. Fedorov, D. Martyshkin, S. Mirov, and V. Gapontsev, Optica **6**, 126 (2019).
17. V. E. Leshchenko, B. K. Talbert, Y. H. Lai, S. Li, Y. Tang, S. J. Hageman, G. Smith, P. Agostini, L. F. DiMauro, and C. I. Blaga, Optica **7**, 981 (2020).
18. S. Vasilyev, I. Moskalev, V. Smolski, J. Peppers, M. Mirov, S. Mirov, and V. Gapontsev, in *Advanced Solid State Lasers* (Optica Publishing Group, 2018), pp. AW3A–1.
19. N. Nagl, in *A New Generation of Ultrafast Oscillators for Mid-Infrared Applications* (Springer, 2021), pp. 35–70.
20. I. T. Sorokina and E. Sorokin, Appl. Phys. Lett. **80**, 3289 (2002).
21. S. Qu, M. Pötzlberger, A. Sebesta, V. Pervak, F. Krausz, A. Weigel, and K. F. Mak, in *CLEO/Europe-EQEC* (Optica Publishing Group, 2021), pp. 1.
22. S. Backus, M. Kirchner, C. Durfee, M. Murnane, and H. Kapteyn, Opt. Express **25**, 12469 (2017).
23. R. Springer, I. Alexeev, J. Heberle, and C. Pflaum, J. Opt. Soc. Am. B **36**, 717 (2019).
24. V. Pervak, T. Amotchkina, D. Hahner, S. Jung, Y. Pervak, M. Trubetskov, and F. Krausz, Opt. Express **27**, 34901 (2019).
25. I. T. Sorokina, E. Sorokin, S. Mirov, V. Fedorov, V. Badikov, V. Panyutin, and K. I. Schaffers, Opt. Lett. **27**, 1040 (2002).
26. P. Dutta and P. Horn, Rev. Mod. Phys. **53**, 497 (1981).
27. C. C. Harb, T. C. Ralph, E. H. Huntington, D. E. McClelland, H.-A. Bachor, and I. Freitag, J. Opt. Soc. Am. B **14**, 2936 (1997).
28. Y. Wang, T. T. Fernandez, N. Coluccelli, A. Gambetta, P. Laporta, and G. Galzerano, Opt. Express **25**, 25193 (2017).
29. S. O. Leonov, Y. Wang, V. S. Shiryaev, G. E. Snopatin, B. S. Stepanov, V. G. Plotnichenko, E. Vicentini, A. Gambetta, N. Coluccelli, C. Svelto, P. Laporta, and G. Galzerano, Opt. Lett. **45**, 1346 (2020).
30. N. Coluccelli, M. Cassinerio, P. Laporta, and G. Galzerano, Opt. Lett. **37**, 5088 (2012).
31. A. Barh, BÖ Alaydin, J. Heidrich, M. Gaulke, M. Golling, C. R. Phillips, and U. Keller, Opt. Express **30**, 5019 (2022).
32. S. Aboujja, D. Chu, and D. Bean, in *High-Power Diode Laser Technology XX*, vol. 11983 (SPIE, 2022), pp. 196–207.